Journal of Electronic Materials, Vol. 6, No. 6, 1977

ANALYSIS OF THE SOLIDUS LINES FOR PbTe AND SnTe

R. F. Brebrick

Metallurgy and Materials Science Program
Marquette University
Milwaukee, Wisconsin 53233

(Received April 22, 1977)

Experimental values of p-n, P_{Te_2}, and T along the solidus lines of PbTe and SnTe, and for compositions within the homogeneity range of SnTe are fit using the simple model of a nondegenerate semiconductor compound containing fully-ionized native defects. As a result values for the intrinsic material parameters of these compounds at high temperature are obtained as well as some indication of the uncertainty in these.

Key words: PbTe, SnTe, defect analysis, intrinsic carrier concentration, intrinsic partial pressure, Schottky constant.

Introduction

There is considerable data for PbTe (1,2) and SnTe (3,4) in the form of the partial pressure of Te_2 and the electronic carrier concentration along the solidus lines. For SnTe the solidus lines have also been established in terms of atom fraction, x, and the relationship between P_{Te_2}, x, and temperature has been established within the solidus field itself (4). However until now these data have not been analyzed to yield the intrinsic parameters for the compound semiconductors. The results

are not as unambiguous for PbTe as might be hoped in that the state of ionization of the native defects cannot be conclusively established from the analysis itself and only a range can be fixed for each of the intrinsic parameters. Nevertheless the results are useful in that the ranges are generally small, except that of the intrinsic carrier concconcentration for the assumption of singly-ionized native defects. Moreover, they should prove helpful in guiding further experiments to characterize the defect state more closely.

The analysis here differs from earlier ones (5,6,32) for PbTe in that we take the data along the solidus lines as most reliable and generally reject data for compositions within the solidus field. An approach similar to ours, but not quite as extensive in the data covered or the analysis itself, was used some time ago by Bis (7).

Model for the Compound Semiconductor

The compounds are assumed to be nondegenerate semiconductors with a native donor and acceptor that are always completely ionized to the same stage z, where z is 1 or 2. The assumption of complete ionization is consistent with the fact that carrier freeze-out is not observed in PbTe and SnTe. Recent ion implantation studies indicate that doubly-ionized Pb and Te vacancies are the predominant point defects in PbTe (8). For completeness, and because all the previous data indicate the defects in the Pb-salts are singly-ionized, we also consider this possibility. Tin telluride is always Te-rich and p-type and the predominant Sn-vacancies have been established to be doubly-ionized (9,10). The relevant behavior of the model can be concisely described (11,12) by an equation connecting the chemical potential of Te, μ_{Te}, and the difference in the concentrations of holes and electrons, p-n, given by

$$\mu_{Te} = \mu_{Te}(\text{int.}) + z\,RT \sinh^{-1}\left(\frac{p-n}{2n_i}\right) + RT \sinh^{-1}\left(\frac{p-n}{2zk_s^{1/2}}\right) \qquad (1)$$

where μ_{Te}(int.) is the chemical potential of Te in an intrinsic (n=p), pure crystal, n_i is the intrinsic carrier concentration whose square is equal to the product of the electron and hole concentrations, z is the degree of ionization and is either 1 or 2 here, and k_s is the product of the concentrations of z-ionized native acceptors (metal vacancies) and z-ionized native donors (Te-vacancies or metal interstitials). Because of the assumption of symmetrical and complete ionization of the native defects, the net hole concentration is related to the difference in the concentrations of native point defects. To be concrete we take these as vacancies and write

$$p-n = z\{[V_M^{-z}] - [V_{Te}^{+z}]\} \tag{2}$$

For the relatively low pressures and high temperatures involved here the vapor phase can be taken as ideal so that the chemical potential of Te and the partial pressure of Te_2, P_2, are related by

$$\mu_{Te} = \mu_{Te}(int) + 1/2\ RT\ \ln\ (P_2/P_2(int)) \tag{3}$$

Using Eq. (3) for the difference in chemical potentials in Eq. (1) gives

$$\ln P_2 = \ln P_2(int) + 2z \sinh^{-1}\left(\frac{p-n}{2n_i}\right) + 2 \sinh^{-1}\left(\frac{p-n}{2zk_s^{1/2}}\right) \tag{4}$$

This equation allows a calculation of p-n for given P_2, or conversely, provided the three basic intrinsic parameters, P_2(int), n_i, and k_s are known. Here these parameters are assumed to depend exponentially upon temperature so that 6 constants must be determined by a fit to the data. Recently (13) an alternate form of Eq. (4) has been obtained for z = 1 in which p-n is given as an explicit function of P_2/P_2(int). In Appendix A we show this alternate equation can be derived from Eq. (4) if z = 1 and that a quartic equation in p-n is obtained when z = 2.

A number of relations that prove useful in discussing our results are now obtained. When the absolute value of p-n is about 3 or more times larger than both $2n_i$ and $2zk_s^{1/2}$, the inverse hyperbolic sine terms each reduce to the logarithm of twice the argument of the sine terms and Eq. (4) becomes

$$\ln(|p-n|) = \frac{\pm 1}{2(z+1)} \ln(P_2/P_2(int)) \pm \frac{z}{(z+1)} \ln n_i \pm \frac{1}{(z+1)} \ln(zk_s^{1/2}) \quad (5)$$

where the upper sign is to be taken for p-n > 0 and the lower sign for p-n < 0. The extrinsic behavior described by Eq. (5) produces two straight lines of slope $\pm 1/2(z+1)$ on a log ($|p-n|$) vs log P_2 plot. At $P_2 = P_2(int)$ these intersect at a value of $|p-n|$ given by

$$|p-n|^* = (n_i^z zk_s^{1/2})^{1/(z+1)} \quad (6)$$

The use of Eq. (5) and (6) is useful in establishing when the theoretical isotherms of p-n vs P_2 given by Eq. (4) are in the extrinsic region. Equations (5) and (6) then coincide with the two branches of Eq. (4).

A measure of self-compensation can be defined for n-type material as

$$f = \frac{p}{n-p} = \frac{[V_M^{-z}]}{[V_{Te}^{+z}] - [V_M^{-z}]} \quad (7)$$

where the 2nd equality follows using Eq. (2). When n = 2p, f = 1 and when p << n, f is near zero. Using Eq. (2) and $[V_M^{-z}][V_{Te}^{+z}] = k_s$, the right side of Eq. (7) can be rewritten to give

$$f = 1/2\{-1 + \left[1 + \left(\frac{2zk_s^{1/2}}{n-p}\right)^2\right]^{1/2}\} \quad (8)$$

If n-p in Eq. (8) is replaced by its absolute value, then Eq. (8) also holds for a corresponding measure of self-compensation in p-type material,

$$f' = \frac{n}{p-n} \tag{9}$$

Finally if D^+ is the net concentration of singly-ionized foreign donors present, Eq. (2) for electroneutrality becomes

$$p-n = z\{[V_M^{-z}] - [V_{Te}^{+z}]\} - D^+ \tag{10}$$

and Eq. (4) becomes

$$\ln P_2 = \ln P_2(\text{int}) + 2z \sinh^{-1}\left(\frac{p-n}{2n_i}\right) + 2 \sinh^{-1}\left(\frac{p-n+D^+}{2zk_s^{1/2}}\right) \tag{11}$$

Thus the partial pressure of Te_2 over a doped, intrinsic crystal is given by

$$\ln P_2(\text{int,doped}) = \ln P_2(\text{int}) + 2 \sinh^{-1}\left(\frac{D^+}{2zk_s^{1/2}}\right) \tag{12}$$

Experimental Input

Lead Telluride

Values for the apparent carrier concentration and partial pressure of Te_2 along the solidus lines of PbTe are tabulated as a function of temperature in the first three columns of Tables I and II and are shown as points in Fig. 1. For Pb-saturated PbTe (Table I), the carrier concentrations were obtained from room temperature Hall measurements on small crystals isothermally equilibrated with Pb-rich ingots and then quenched (1). It should be

Table I. Pb-saturated PbTe. Experimental data in Ist three columns. Calculated values of n-p in last column were obtained using parameters of entry 2 in Table IV. Entries with no experimental value of n-p are given to indicate the temperature dependence of n-p more completely.

T °C	10^4 P_{Te_2} atm	10^{-17}(n-p),exp. cm^{-3}	10^{-17}(n-p),cal. cm^{-3}
416.7	$1.73(10^{-10})$	--	0.26
441	$1.01(10^{-9})$	--	0.39
500	$4.42(10^{-8})$	.75, .94	0.93
503	$4.50(10^{-8})$	.98, 1.1	1.05
580	$3.17(10^{-6})$	2.37, 2.46	2.5
582	$3.40(10^{-6})$	2.39	2.6
590	$5.01(10^{-6})$	3.43	2.8
595	$6.90(10^{-6})$	3.35, 3.39	2.85
596	$6.90(10^{-6})$	4.05	2.85
705	$5.40(10^{-4})$	8.79, 9.90	9.19
795	0.013	15.3	16.6
800	0.0148	13.6 , 14.5	17.5
803	0.016	14.2 , 14.5	18.1
814	0.022	--	19.6
826	0.042	--	17.0
838	0.095	--	11.7
844	0.140	--	9.1
850	0.210	6.53, 6.67	5.88
859	0.35	2.2	2.2
876.4	1.0	--	-7.7
884	1.6	-16.4 ,-16.6	-13.4
917.5	12.	--	-49.5

noted that at the highest temperature of 884°C that Pb-saturated PbTe is p-type i.e. $n-p < 0$. The assumption that the high temperature value of n-p is effectively maintained during the quench is supported by experiments with greatly different quench rates, by the temperature dependence of the values themselves, and by annealing studies (14) which show internal precipitation to be slow in Pb-saturated PbTe. The n-type samples are extrinsic, $n >> p$, at room temperature and we take $n-p = -1/eR_{298}$.

Table II. Te-saturated PbTe. Experimental data in 1st three columns. Calculated values of p-n in 4th column obtained using parameters in entry 2 of Table IV. For calculated values of p-n in last column, W and V in entry 2 were replaced by those in Eq. (27). Entries with either P_{Te_2} or (p-n), exp. missing were not included in the fitting.

T °C	$10^4 P_{Te_2}$ atm	10^{-18}(p-n) exp.	10^{-18}(p-n) cal.	10^{-18}(p-n) cal.
181	$8.35(10^{-7})$	0.14	0.02	0.19
204	$5.89(10^{-6})$	0.18	0.04	0.23
245	$1.25(10^{-4})$	0.33	0.12	0.33
294	$2.65(10^{-3})$	0.50	0.34	0.44
370	0.10	1.1	1.3	
385	0.21	1.4	1.63	
395	0.30	2.1 v	1.87	
418	0.95	2.58,2.67	2.68	
420	1.0	2.9 v	2.7	
485	3.75	5.6 v	5.1	
497	5.4	6.44,6.6	5.81	
500	5.8	6.7,6.8,6.9	5.97	
575	--	8.8 v	--	
591	2.63	9.0,9.8	11.5	
600	--	10.36,10.40	--	
636	5.20	--	15.1	
679	8.29	--	18.2	
687	--	10.6,11.1 l	--	
703	--	9.2,9.3	--	
727	12.2	--	21.1	
746	--	10.5,11.0 l	--	
788	--	8.1,8.3	--	
796	--	9.5 v	--	
798	--	8.6,8.8,9.3,9.3	--	
838	16.0	--	21.6	
863	14.0	--	19.5	
903.5	8.70	--	14.5	
917.5	5.80	--	11.5	
924	2.89	--	7.88	

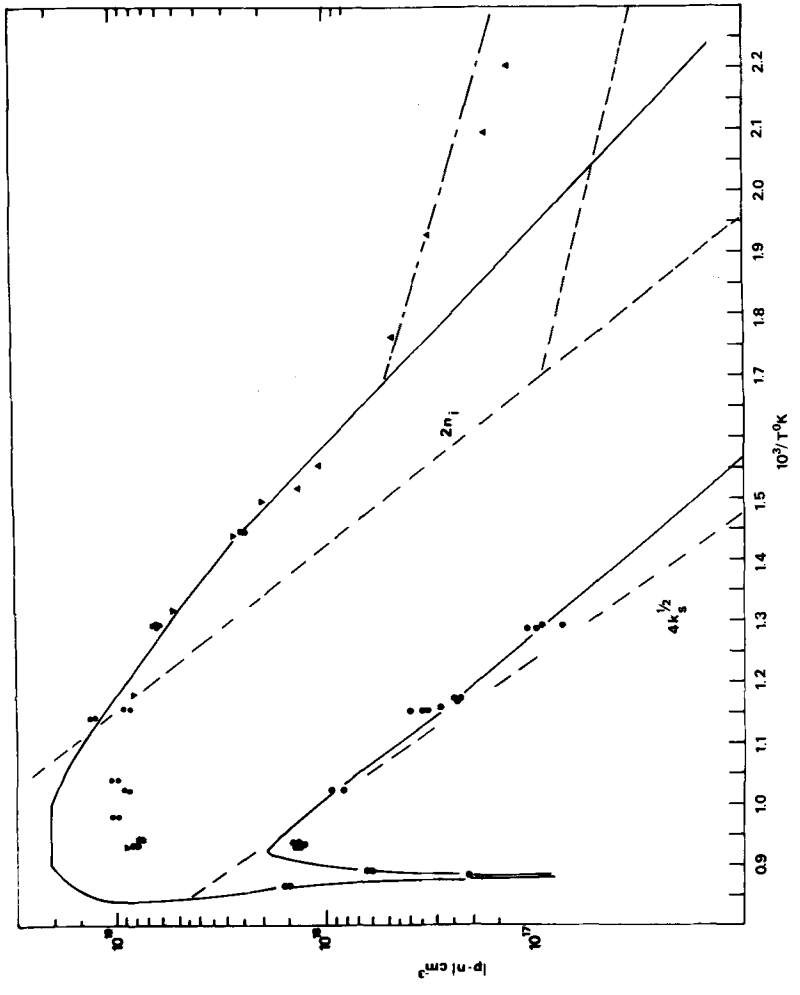

Fig. 1 Absolute value of the net carrier concentration, $|p-n|$ along the solidus lines of PbTe plotted on a log scale vs $10^3/T$. Upper leg is for Te-saturated, p-type PbTe. Bottom leg is for Pb-saturated PbTe; which is n-type for $10^3/T$ greater than 0.875, p-type below. Solid lines were calculated using Eq. (4) and parameters of entry 2, Table IV. Experimental data shown as points. Dot-dash line at lower right shows p-n for Te-saturation if the temperature dependence of n_i is changed below 312°C to that given by Eq. (27).

Tellurium-saturated PbTe was generally obtained in the same manner as Pb-saturated PbTe except that the crystals were equilibrated with a Te-rich ingot containing more than 50 at % Te (1). Not all of the results for T > 600°C are given in Table II because there is evidence that the quench used was not rapid enough above 600°C. Between 600° and 850°C the hole concentrations scatter between $5(10^{18})$ and 1.2×10^{19} cm^{-3}.

Crystals grown from stoichiometric, pure, melts have an apparent hole concentration, $\hat{p}_{298} = 1/eR_{298}$, between 3 and $5(10^{18})cm^{-3}$ and contain a Te-rich microprecipitate. (This precipitate is a result of the retrograde solubility of Te in PbTe(c). It is also present in crystals Te-saturated above 600°C the difficulty of achieving an adequate quench rate attesting to the rapidity of precipitation.) Internal equilibrium between the crystal and precipitate is achieved rapidly because of the short diffusion distances involved and yields reproducible values for the hole concentration as a function of anneal temperature (1,14). The first 6 entires in Table II were obtained by annealing as-grown, p-type crystals under vacuum at 385°C and below (14). Four other hole concentrations were obtained (1) similarly at higher temperatures and are distinguished by the letter v after the concentration. These high temperature results are close to those obtained by equilibrating PbTe with a Te-rich ingot, indicating that at high temperatures the internal microprecipitate behaves thermodynamically just like the bulk, Te-rich liquid phase coexisting with Te-saturated PbTe. It has generally been assumed that this is also true for the vacuum anneals below 385°C. As Fig. 1 shows these points have a distinctly different, weaker dependence on temperature than might be anticipated from the higher temperature results obtained by equilibration with bulk ingots. The four concentrations in Table II followed by the Roman numeral I are from an earlier study (15).

Defining the nominal hole concentration at 77K in terms of the Hall coefficient measured at 77K and 4.5 kG as

$$\hat{p}_{77} = 1/e\ R_{77} \qquad (13)$$

we take the true value of p-n to be given by

$$p\text{-}n = 0.9\ \hat{p}_{77} \tag{14}$$

for values of $\hat{p}_{77}$ between 10^{17} and 10^{19} cm^{-3}. (High field experiments indicate (16) the coefficient is between 0.9 and 1.0.) The data available to us are the nominal hole concentrations at 295K,

$$\hat{p}_{295} = 1/e\ R_{295} \tag{15}$$

The Hall coefficient of p-type PbTe at 77K is smaller than that at 295K and more so the larger $\hat{p}_{295}$, due to the presence of a second valence band. Taking a smooth curve through the data showing this effect (16) and using Eq. (14) we get

$$p\text{-}n = \ell\ \hat{p}_{295} \tag{16}$$

and

$$\ell = 0.255\ \log_{10} \hat{p}_{295} - 3.470 \tag{17}$$

The experimental values of p-n given in Table II were obtained from values of $\hat{p}_{295}$ using Eqs. (16) and (17). When $\hat{p}_{298}$ is $1.85(10^{17})$, p-n is $1.8(10^{17})$. When it is $7.32(10^{18})$, p-n is $9.81(10^{18})cm^{-3}$.

The values given here for n-p of Pb-saturated PbTe at 800°C and 500°C and for $\hat{p}_{295}$ of Te-saturated PbTe at 350°C are in close agreement with recent values obtained by Strauss (17) using the same technique. His value of $\hat{p}_{295} = 4(10^{18})$ for Te-saturation at 800°C is presumably low because of the quench effects known to be important for Te-saturated PbTe above 600°C. In contrast Chou et al (18) obtained $\hat{n}_{298} = 3.5(10^{18})$ for Pb-saturation at 750°C and $\hat{p}_{298} = 1.4(10^{19})$ for Te-saturation at 720°C. The latter result is not inconsistent with the results given here, which represent a lower limit because of quench effects, but the former result is significantly higher. Using the two temperature technique in which PbTe at a high temperature is in vapor contact with a Te or Pb-reservoir at lower temperature, Sato et al. (19)

and, then Fujimoto and Sato (6), obtained carrier concentration vs P_2 isotherms for three temperatures. Their Pb-saturated PbTe was about $5(10^{18})$ at 600°C, significantly higher than our values which show a maximum of about $1.5(10^{18})$ at 800°C and drop rapidly at lower temperatures.* These high values for Pb-saturated PbTe are in rough agreement with an early study (15) which gave a maximum solubility corresponding to $n-p = 3.5(10^{18})$ near 780°C. The subsequent study, whose results are used here, was made on crystals of higher purity and the older crystals were found to contain $1.5(10^{18})cm^{-3}$ of Cu, a known donor in n-type PbTe, by calibrated emission spectroscopy. The contradictory findings are therefore ignored here.

The partial pressure of Te_2 over Te-saturated PbTe has been determined by measurement of the vapor optical absorbance (1) between 596° and 924°C and by a visual, two-temperature method (20) between 550° and 900°C. The results agree to better than 10%.** More recently we have employed the optical absorbance method to establish P_2 over a lower temperature range between 352° and 545°C using the strongly absorbing (21) $Te_2(g)$ peaks at 1995 and 2025Å. The partial pressures coincide to better than 3% with those of pure Te(s) below a eutectic temperature measured as 421.4°C. When linearly extrapolated to high temperature on a log P_2 vs $10^3/T$ plot they agree with the earlier results. Above 421°C smoothed values of P_2 were read for each of the temperatures in Table II. At lower temperatures the published vapor pressure of Te(s) was used (22).

Values of P_2 over Pb-saturated PbTe below 820°C were calculated from the vapor pressure (22) of pure Pb and the Gibbs free enthalpy of formation of PbTe, in effect assuming that PbTe is essentially in equilibrium with pure Pb below 820°C. The equations used are

$$\ln P_2(\min) = 2\Delta G_f^o/RT - 2 \ln P_{Pb}^o \qquad (18)$$

*High values for Pb-saturated PbTe are also reported in Ref. 32. An English summary appears in Ref. 33.

**A total pressure measurement (34) for Te-saturated PbTe is in fair agreement near 800°C but significantly higher at lower temperatures.

where P^{o}_{Pb} is the vapor pressure of Pb and ΔG^{o}_{f} is for the reaction

$$Pb(g,1\ atm) + 1/2Te_2(g,1\ atm) = PbTe(c) \qquad (19)$$

Based upon emf measurements (23) between 350° and 480°C and published data for the heat of fusion and melting point (22) for Pb and Te, ΔG^{o}_{f} is given by

$$\Delta G^{o}_{f} = -79,322.9 + 41.519T\ cal/mol \qquad (20)$$

Values of P_2 for Pb-saturated PbTe between 820° and 924°C were obtained by plotting the data between 883° and 924°C on a log P_2 vs $10^3/T$ scale and drawing the best straight line. This intersects the P_2(min) line at 820°C.

Tin Telluride

It has been established (9,10) that the hole concentration in SnTe, which is always Te-rich and p-type, is given in terms of the Hall coefficient at 77K by

$$p = 0.63/eR_{77} \qquad (21)$$

Since p >> n at 77K for the samples measured, we take p-n $\approx$ p for use in Eq. (4). Values of p for both Sn- and Te-saturated SnTe are given as a function of temperature in Table III. The first 9 entries are from Houston and Allgaier (10,24) (numerical values were kindly furnished by Dr. Houston). The remaining entries in Part A and the 1st 6 in Part B for Te-saturation are from isothermal annealing experiments (3) similar to those described for PbTe. In addition partial pressure measurements have been made on known compositions within the homogeneity range of SnTe (4). Values of p-n for these samples can be calculated as follows. The predominant atomic point defects are Sn-vacancies. The number of these per cm^3, V_{Sn}, is related to the atomic fraction of Te by

$$V_{Sn} = 6.32(10^{22})(x_{Te}-1/2) \qquad (22)$$

Table III. SnTe 10th and 1st three entries omitted from fit.

	$10^3/T$	$10^5 P_{Te_2}$ (atm)	10^{-20}(p-n),exp.	10^{-20}(p-n),cal.
A.	Sn-saturated			
1.	1.485	$1.9(10^{-7})$	0.422,0.454	0.221
	1.375	$5.8(10^{-6})$	0.53	0.38
	1.38	--	0.55,0.586	--
	1.295	$7(10^{-5})$	0.63,0.68	0.54
	1.210	$1(10^{-3})$	0.84,0.913	0.84
	1.145	$8(10^{-3})$	1.05,1.11	1.17
	1.090	$4.5(10^{-2})$	1.5	1.52
	1.088	$4.7(10^{-2})$	1.4	1.53
	1.080	$6.0(10^{-2})$	1.35	1.58
10.	1.215	$1.07(10^{-3})$	2.0,2.0, 2.15	--
	1.032	0.289	1.85,1.99,2.16	2.04
	1.0213	0.421	1.78,1.92	2.18
	1.0203	0.421	1.84,2.19	2.17
	.9813	1.91	3.45,3.89	2.87
	.9803	2.00	2.40,2.41	2.90
	.9569	6.0	2.83,3.12	3.62
	.9420	12.3	3.94,4.26	4.18
B.	Te-saturated			
	1.2149	72.4	10.9	11.0
	1.0214	316	9.6	11.0
	1.0172	316	9.48	10.9
	.9793	263	9.92	9.84
	.9578	192	8.69,8.88	8.78
	.9341	92.1	6.27	6.94
	1.2003	84.2	11.1	11.1
	1.1506	141	11.1	11.4
	1.1000	230	11.4	11.7
	1.0503	303	11.1	11.4
	.9999	303	10.5	10.5
	.9746	250	9.86	9.63
	.9774	260	10.1	9.77
	.9559	184	8.85	8.66
	.9398	121	7.58	7.53
	.9276	57.9	6.32	6.05
	.9267	39.5	5.06	5.45

where the number of sites in each sublattice of the NaCl structure is taken as equal to the room temperature value. This was calculated from the measured lattice parameter (9) and varies by less than 5% over the homogeneity range. On the other hand each Sn-vacancy is assumed to be doubly-ionized i.e.

$$p = 2V_{Sn} \tag{23}$$

Extrapolating the log P_2-$10^3/T$ measurements to intersection with the measured three-phase curve gives solidus points. If the composition in atomic fraction is converted to hole concentration using Eqs. (22) and (23), the results are in close agreement with those obtained from Hall measurements on quenched samples using Eq. (21). This is shown in Fig. 4 where the experimental values of p-n along the SnTe solidus lines are shown as points. The last 5 entries of Part B, Table III were obtained as described above. Entries 7 through 12 in Part B were obtained by constructing isotherms of p-n vs tellurium pressure on a log-log scale and extrapolating these to the Te-saturation pressure.

The partial pressure of Te_2 has been determined from optical absorbance measurements (4) between 500° and 806°C for Te-saturated SnTe and between about 700° and 806°C Sn-saturated SnTe. The entries in Table III for these temperature ranges are from a smoothed curve through generally closely-spaced, tightly clustered points. The minimum partial pressure of Te_2 over SnTe, $P_2(min)$, was calculated from the vapor pressure of Sn (22) and the standard Gibbs free enthalpy of formation, ΔG_f^o, of SnTe(c) from Sn(g) and Te_2(g) using an equation similar to Eq. (18). The equation used for ΔG_f^o is

$$\Delta G_f^o = -101{,}300 + 43.36T \text{ cal/mol SnTe(c)} \tag{24}$$

and is based upon the published heats of fusion and melting points (22) of Sn and Te and emf measurements (23) between 260° and 395°C. We obtain

$$\log_{10} P_2(min,atm) = -13.802(10^3)/T + 8.701 \tag{25}$$

The measured values of P_2 for Sn-saturated SnTe are, as demanded by thermodynamic self-consistency, higher than those calculated using Eq. (25) and when extrapolated to low temperatures intersect the P_2(min) line at 732°C. Therefore for temperatures below 732°C ($10^3/T = 0.995$), the values of P_2 in Table III for Sn-saturated SnTe were obtained using Eq. (25). The measured values of P_2 for Sn-saturated SnTe are the smallest measured, and as shown in the original investigation, are subject to an uncertainty of perhaps $\pm$ 100%.

The value of P_2 along the SnTe three phase curve is shown in Fig. 5. The points shown are the experimental values for various compositions within the SnTe homogeneity range.

Analysis and Results for PbTe

Values of the intrinsic parameters were sought which minimized a measure of fit, σ, whose square was defined as:

$$\sigma^2 = \sum_{i=1}^{N} [\ln (p-n)_{i,cal} - \ln (p-n)_{i,exp}]^2/N \qquad (26)$$

where $(p-n)_{i,cal}$ was obtained by solving Eq. (4) for given P_2,T, and given values of the intrinsic parameters using a trial and error search technique (25). Thrity-nine experimental triplets of P_2, p-n, and T were used. Points corresponding to Te-saturation at 600°C and above were not included in the fit for reasons cited and four points corresponding to Te-saturation below 370°C were also omitted because their inclusion significantly deteriorated the measure of fit. This point is taken up again in the Discussion. The value of σ was computed for some starting values of the six intrinsic parameters and then these were varied in a second trial and error search subroutine to find a minimum value for σ. The σ-surface in the six-dimensional space of the intrinsic parameters is not deep or sharply curved in the neighborhood of the minimum. Instead it is relatively flat and, especially for z = 1, covers an extensive range with only a small increase in σ. To give some idea of this behavior, entries are given in Table IV which give the minimum σ for fixed W, the

Table IV. PbTe, 39 points. Omit Te-saturation data above 591 and below 370°C in fit.
$\log_{10} n_i = W/T + A$; $\log (2zk_s^{1/2}) = C/T + D$; $\log P_2(\text{int,atm}) = V/T + B$

Nbr	z	W	A	C	D	V	B	σ	$(p-n)(10^{-18})$ cm^{-3} at Max	at 924°C	at 181°C	n_i at 25°C
1	2	-3300	22.36	-4151	22.21	-14560	8.461	.16	19.	7.9	.038	$2(10^{11})$
2	2	-3700	22.99	-4191	22.19	-14250	8.197	.15	23.	7.9	.020	$3.7(10^{10})$
3	2	-4200	23.78	-4247	22.19	-13860	7.856	.16	27.	7.7	.009	$4.8(10^{9})$
4	1	-600	19.52	-5710	23.60	-12040	6.235	.161	17.	8.8	.007	$3.2(10^{17})$
5	1	-1100	20.04	-5503	23.37	-12130	6.327	.159	17.	8.5	.013	$3(10^{16})$
6	1	-1450	20.41	-5403	23.26	-12230	6.418	.163	17.	8.3	.018	$3.5(10^{15})$
7	1	-3000	22.22	-5007	22.86	-12600	6.746	.145	21.	8.6	.020	$1.4(10^{12})$
8	1	-3500	22.80	-4885	22.74	-12760	6.892	.144	23.	8.4	.015	$1.1(10^{11})$
9	1	-4000	23.40	-4747	22.61	-12890	7.004	.148	25.	8.2	.011	$9(10^{9})$

parameter determining the temperature dependence of n_i (see heading for Table IV).

Entry 2 is the best fit for z = 2. Although σ is increased only slightly for entries 1 and 3, it starts to increase rapidly for values of W further removed from -3700. For z = 1, the minimum in a σ vs W plot is very shallow and there is no significant increase in σ over the extended range in W shown by entries 4 through 9. However, at W = -4500, σ does start to increase and is 0.158 and 0.172 at, respectively, W = -4500 and -5000. Because of the symmetry of Eq. (4) with z = 1 as regards $2n_i$ and $2k_s^{1/2}$, identical fits can be obtained for each entry by interchanging the numerical values of W and C, replacing A by D-log 2, and replacing D by A+log 2.

All the entries shown, both for z = 2 and z = 1, fit the data essentially equally well. The solid line shown in Fig. 1 is for entry 2, z = 2, and W = -3700 as are the calculated values for p-n in Tables I and II. It is seen the fit is good even near $10^3/T = 0.875$ where n-p for Pb-saturated PbTe abruptly changes sign. The other entries give fits that are only slightly different as shown in part in the last columns of Table IV. None of the entries fit the data for Te-saturation below 370°C well, the discrepancy increasing with decreasing temperature. For z = 2, the extrapolated values of n_i at 25°C are much below the best present estimate (26,27) of $3\text{-}5(10^{15})cm^3$. For z = 1, the extrapolated values of n_i are much closer and that for entry 6, W = -1450 is in essential agreement.

Even though the individual parameters differ significantly for the various entries in Table IV, the corresponding differences between $k_s^{1/2}$ and $P_2(int)$ are generally small in the high temperature range. For z = 1 the values for $P_2(int)$ are essentially the same at 924°C and are all within a factor of 2 at 600°C. Those for z = 2 fall within this same range. Thus in spite of the wide range in the values of W giving good fits, and the ambiguity associated with obtaining equally good fits of 14 to 16% with two possibilities for the ionization state of the native defects, $P_2(int)$ is fairly closely defined. A similar result is obtained for the Schottky constant. For z = 2 the values of $k_s^{1/2}$ are within 20% of one another between 500° and 924°C whereas for z = 1 they are all

within a factor of 1.6 of another over the same temperature range. The quantities that enter Eq. (4) are $4k_s^{1/2}$ for z = 2 and $2k_s^{1/2}$ for z = 1. The quantities that enter Eq. (4) are $4k_s^{1/2}$ for z = 2 and $2k_s^{1/2}$ for z = 1. At 924°C the values of $4k_s^{1/2}$ for entries 1 through 3, z = 2, fall within the narrow spread of values of $2k_s^{1/2}$ for entries 4 through 9, z = 1. At 500°C the values of $4k_s^{1/2}$ for z = 2 are 3.5 or less times as large as the values of $2k_s^{1/2}$ for z = 1. The spread in the values of $2n_i$ is greater covering a factor of 3 between 181° and 924°C for z = 2. For z = 1 all six entries give about the same value for $2n_i$ at 600°C. However at 924° and 441°C the values associated with the different entries in Table IV differ by a factor of about 10. Of particular note is the fact that the value of $2n_i$ calculated using band parameters established below room temperature (27) (see Eq. 28) is 10^{17} at 127°C and $6.8(10^{17})$ at 924°C and above 127°C is lower than those for all of the entries in Table IV, at high temperature by a factor of 10 to 100.

Discussion for PbTe

Between 500° and 800°C the values of $4k_s^{1/2}$ for z = 2 are about 1/2 to 1 times the value of n-p for Pb-saturated PbTe, whereas the values of $2k_s^{1/2}$ for z = 1 are about 1/5 to 1 times the value of n-p. In both cases the near equality occurs near 800°C. Therefore according to Eq. (8), the measure of self-compensation lies between 0.01 and 0.2 and is substantial.

On the basis of the fits to the values of p-n along the PbTe solidus lines given in Table IV two choices seem available:

1. If z is taken as unity, then entry 6 seems the best fit on the basis of value of n_i it gives at 25°C. The failure to fit the Te-saturated data below 370°C would then have to be explained. One possibility would be to postulate that the internal microprecipitate is subjected to an increasing strain, and hence increased chemical potential of Te, as the temperature is lowered below the PbTe-Te eutectic temperature of 421°C.

11. On the other hand, if z is taken as 2 in accordance with the recent ion implantation studies (9), then entry 2 gives the best fit. However one is then forced to assume a rapid change in the temperature dependence of n_i beginning near 370°C so that a value near $3(10^{15})cm^{-3}$ is obtained at room temperature.

Assuming this change consists of a discontinuity in the slope of n_i at 312°C, then below this temperature n_i is given by:

$$\log n_i = -725.4/T + 17.91 \qquad (27)$$

The values calculated using Eq. (27) differ by less than 5% from those given by an expression based upon the low temperature band parameters in Dalven's review (27) and given by

$$\log n_i = -453.5/T - 1.058 + 1.5 \log T + 14.36 \qquad (28)$$

Adoption of Eq. (27) not only gives a correct value of n_i at 25°C with a temperature variation of n_i that is close to that expected up to 312°C, it also results in a greatly improved fit to the Te-saturated data below 370°C as shown by the dashed line near these points in Fig. 1. (The values for $k_s^{1/2}$ and $P_2(int)$ used are from the high temperature fit listed under entry 2 in Table IV.) As a result there is no necessity to assume the internal microprecipitate in Te-rich PbTe is significantly different than the bulk phase coexisting with Te-saturated PbTe.

Recent experiments (28) in which PbSe crystals were grown from material of known carrier concentration with known additions of Pb or Se give the result that for both n and p-type PbSe,

$$z/r = 2.0 \pm 0.4$$

where r is the proportionality constant between the hole or electron concentration and $1/eR_{77}$ and is expected to be near unity. This and the recent results cited for PbTe (8) are in contrast to the interpretation of experiments which measured the isothermal dependence of p-n

upon partial pressure in the Pb-salts. Bloem and Kroger (29) and more recently, Harman and Strauss (13) obtained z = 1 for PbS. Measurements by two groups have given a similar result for PbSe (30,31). Finally, Fujimoto and Sato (6), have obtained z = 1 for PbTe. As pointed out in the section on Experimental Input, the latter experiments give values of n-p for Pb-saturated PbTe that are about $2(10^{18})cm^{-3}$ higher than those used here. Figure 2 shows theoretical plots of log ($|p-n|$) vs log P_2(atm) at 600°C as well as the experimental data (19) as points. The uppermost solid curve at high pressures is for entry 2, z = 2. The solid curve below it is for entry 6, z = 1. Both curves agree quite closely at the Pb- and Te-saturation limits indicated by the vertical bars. The dashed straight lines are the extrinsic lines for each case as given by Eq. (5). These show that even at Te-saturation extrinsic behavior has not been reached. It can be seen that a straight line does give a good approximation to the theoretical curve for z = 2 above about $3(10^{18})cm^{-3}$. Its slope, however, is much closer to the value of 1/4 expected for extrinsic behavior when z = 1 than it is to the extrinsic slope of 1/6 for z = 2. Sato's (19) p-type points are generally closer to the curve for z = 2 except for the highest point, which could be low because of inadequate quenching. The theoretical curve generated by Fujimoto and Sato's (21) intrinsic parameters and z = 1 goes through their two highest n-type points at $2.8(10^{18})$ and $1.1(10^{18})$ but falls below all their p-type points by about 10^{18} in p-n. (At 750°C the intrinsic parameters of these authors fit the p-type points quite well.)

Gas'kov et al (32,22) also determined isotherms of p-n vs P_2 using the two temperature technique. Their data for n-type PbTe are not in good agreement with theoretical curves generated using the parameters of either entry 2 or 6 of Table IV. In part the discrepancy arises because they obtained higher values of n-p than the value we use for Pb-saturated PbTe. In part it arises because they use an expression for the free energy of formation of PbTe different than Eq. (20) and so obtain a higher calculated value of P_2 for given Pb-reservoir temperature and P_{Pb}. Their experimental isotherms of p-n vs P_2 for Te-rich PbTe (obtained using a Te reservoir) are in fair agreement with those calculated using the parameters of entry 2, Table IV, for z = 2. The agreement is good

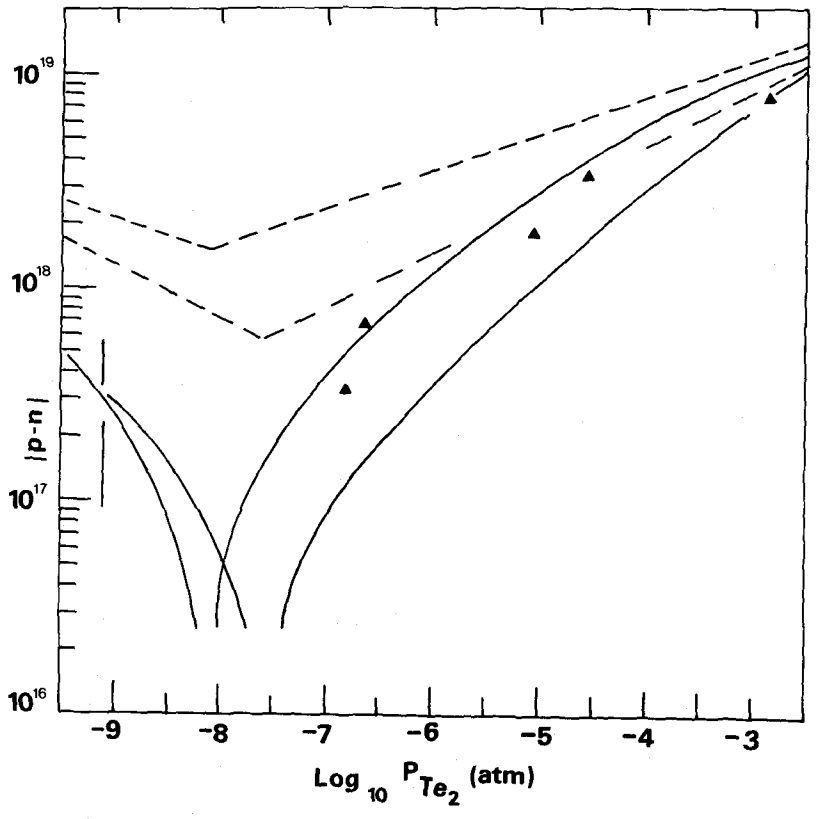

Fig. 2 Isotherms at 600°C for PbTe of the absolute value of p-n versus Te_2-partial pressure in atm, both plotted on a log scale. Calculation for doubly-ionized defects using parameters of entry 2, Table IV, gives the solid line that is uppermost at the highest pressures. The other solid line is for singly ionized defects using entry 6 of Table IV. Triangles are experimental points from Ref. 19. Vertical bar indicates the pressures at Pb-saturation. Te-saturation is at -2.53, close to right vertical axis. Dashed lines are extensions of hypothetical extrinsic behavior, as given by Eqs. (5) and (6), into the homogeneity range of PbTe.

for the lowest isotherm at 645°C and poorer at higher temperatures. In general the experimental values of p-n occur at lower values of P_2 than given by the theoretical curves.

It is our belief that the weight of experimental evidence lies in favor of z = 2 for PbTe. Further experimental confirmation relying upon the establishment of p-n vs P_2 isotherms would have to be fairly precise to be unambiguous. It seems to us that such experiments would best be carried out a) on the Te-rich side where there is a greater range of p-n values to be covered and where P_2 could be established directly, b) at temperatures below 600°C so that quenching would not be a problem, and c) for some small range of donor concentrations in the 10^{18} range. To illustrate the differences that might be expected, Fig. 3 shows theoretical isotherms at 500°C for both z = 2 and z = 1 and for both pure PbTe and PbTe with $4(10^{18})$ singly-ionized foreigh donors. The vertical bars represent the stability limits for pure PbTe (2).

As mentioned before, previous analyses have used data for Pb-rich PbTe(c) that are inconsistent with those used here. Nevertheless it is of interest to compare the values obtained for the intrinsic material parameters. Since analytical expressions were not always given for these, the comparison is made by giving values of the parameters at two temperatures in Table V. In general the values from the different investigations for each parameter are relatively close. However the values of $2n_i$ from this work are consistently the largest. It should be noted that the model used in Ref. 33 is more complicated than those of the remaining studies in ascribing a non-zero ionization energy to the native donor and acceptor levels.

Analysis and Results for SnTe

As shown in Fig. 4, p-n for Sn-saturated SnTe has a distinctly shallower slope at the lowest temperatures than at the higher ones. For this reason the experimental values at the two lowest temperatures (first two entries in Table III) were omitted from the fit, leaving 75 experimental points. Using the measure of fit, σ, defined by Eq. (26) it was again found that the minimum in the σ surface was very shallow. Therefore, as in the case of PbTe, fixed values of W were chosen in the vicinity of

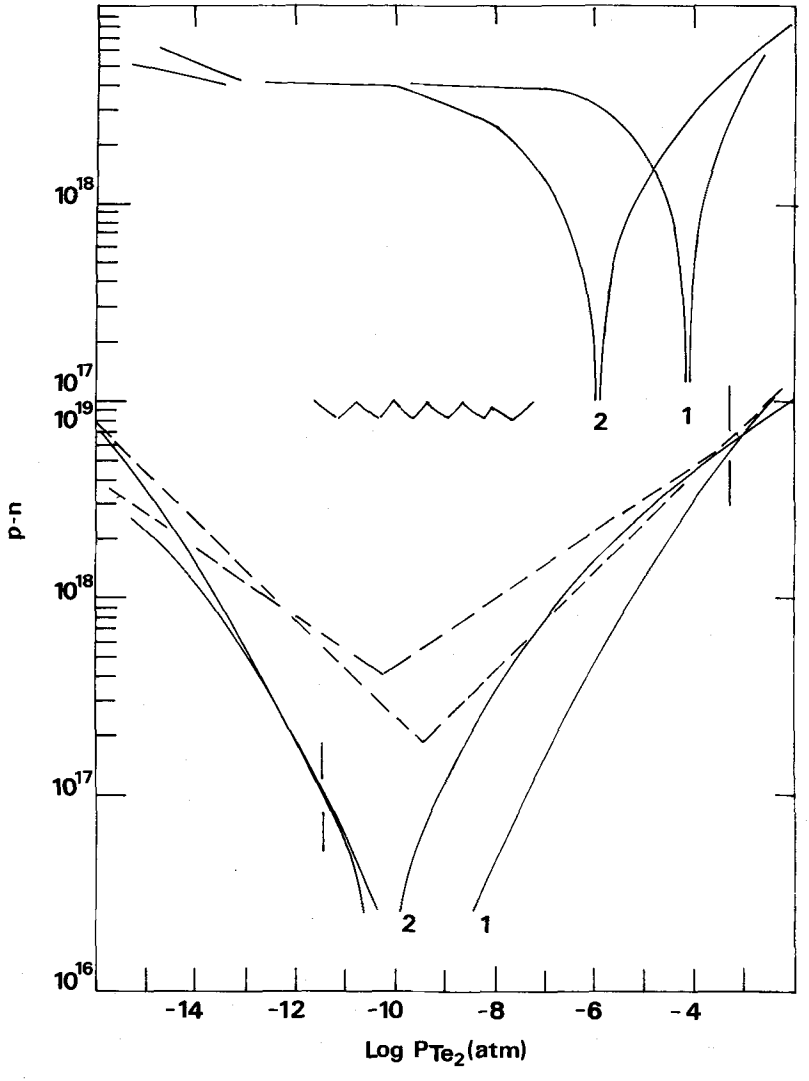

Fig. 3 Isotherms of |p-n| vs P_{Te_2} for PbTe at 500°C on a log-log plot. The lower half of the figure shows calculated isotherms as solid lines. Curve 2 is for z=2, entry 2 of Table IV; curve 1 is for z=1, entry 6 of Table IV. Vertical bars at -11.45 and -3.24 indicate the experimental pressure limits of the PbTe homogeneity range. The dashed lines are extrapolations of the extrinsic lines

given by Eq. (5). The upper half of the figure shows calculated isotherms for PbTe containing $4(10^{19})$ singly-ionized, foreign donors per cm^3.

Table V. Comparison of intrinsic material parameters for PbTe from various sources.

T (°K)	z	$2n_i \times 10^{-18}$ (cm^{-3})	$2zk_s^{1/2} \times 10^{-18}$ (cm^{-3})	$P_2(int) \times 10^8$ (atm)	Ref.
873	1	3.6	0.6	~4	5
	1	3.6	0.73	3.	6
	1	1.3	$3.8(10^{-4})$	2.2	33
	1	11.0	0.12	2.6	Here
	2	11.0	0.25	0.75	Here
	2	3.6	0.24	~4	5
1023	1	9.2	4.0	--	5
	1	9.8	3.4	200	6
	1	3.3	$2.9(10^{-3})$	420	33
	1	20.0	0.95	290	Here
	2	47.0	1.2	190	Here
	2	9.2	16.0	--	5

the minimum and the other parameters varied to reach a constrained minimum. The results in Table VI show that essentially equal measures of fit are obtained over a wide range of W values around the value of about -2152 giving the very best fit. Although the temperature dependence of the material parameters $2n_i$, $4k_s^{1/2}$, and $P_2(int)$ are generally not closely defined as a result of the fit, the parameters themselves are fairly closely fixed. Between 500° and 806°C all entries in Table VI give values for $2n_i$ that are the same within a factor of 2, values for $4k_s^{1/2}$ that are the same within a factor of 4, and values for $P_2(int)$ that are the same within a factor of 5 except for that corresponding to entry 2, which is higher by about a factor of 10. We believe entry 3 to give the best fit in the following sense. Although it is not quite as good as entry 2 in fitting the Sn-saturation points at low temperature, it is best in fitting the experimental

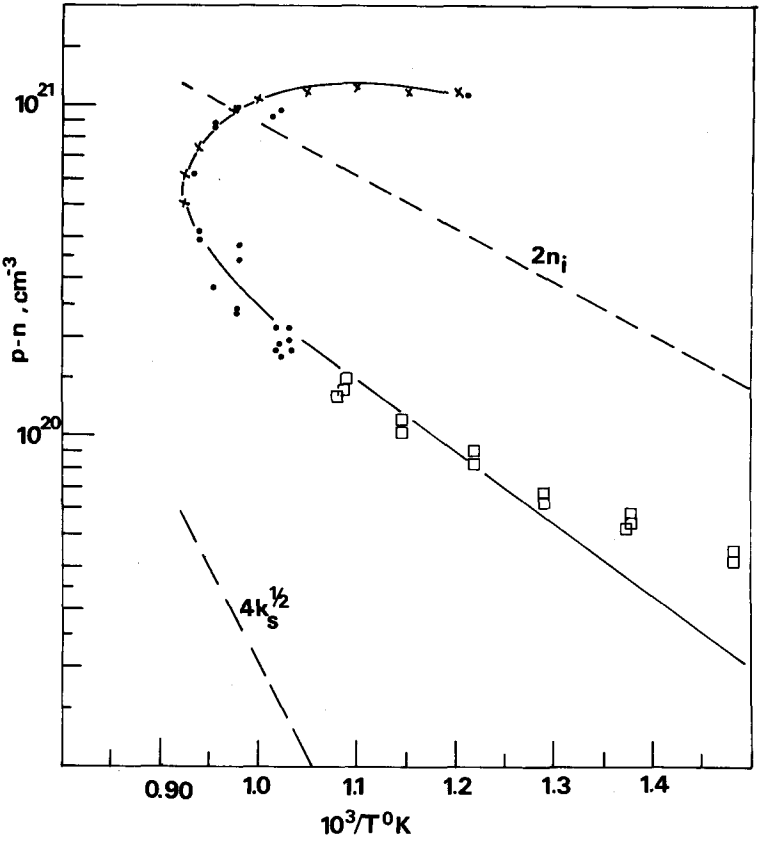

Fig. 4 The net carrier concentration p-n along the solidus lines of SnTe plotted on a log scale vs $10^3/T$. Solid line is calculated using the parameters of entry 3, Table V. Experimental data are shown as points.

Squares: Houston, Ref. 10
Filled Circles: Ref. 3
X : Ref. 4

partial pressures for compositions within the homogeneity range. The calculated values of p-n in Table III as well as the solid curves in Fig. 4 and Fig. 5 were obtained using the parameters in entry 3. Fig. 5 shows the data

Table VI. SnTe, z=2. 75 points. Omit Sn-saturated data at two lowest temperatures from Ref. 10,24. $\log_{10} n_i = W/T + A$; $\log(4k_s^{1/2}) = C/T + D$; $\log P_2(\text{int,atm}) = V/T + B$

Nbr	W	A	C	D	V	B	σ	n_i(25°C)
1	-2700	23.44	-5239	24.77	-21370	13.70	.0999	$2.4(10^{14})$
2	-2152	22.85	-5426	25.31	-20810	13.76	.0926	$4.3(10^{15})$
3	-1600	22.24	-5597	24.92	-20120	11.83	.0946	$7.4(10^{16})$
4	-1400	22.03	-5511	24.87	-20030	11.83	.0958	$2.1(10^{17})$

for 50.8, 50.7, and 50.6 at % Te are fit almost exactly. The calculated P_2-values for 50.5 and 50.4 at % Te are all somewhat high compared to the experimental points. The experimental P_2-values for these latter compositions are among the lowest measured and could be somewhat in error.

Discussion for SnTe

Entry 3 in Table VI, our final choice for the best fit to the SnTe data, gives an extrapolated value of $7.4(10^{16})$ for n_i at 25°C. The calculated value of p-n for Sn-saturated SnTe in the 400° to 500°C region is insensitive to the value of $2n_i$. Assuming $2n_i$ at 400°C is doubled to $3(10^{20})$, only increases p-n for Sn-saturation at 400°C from $2.2(10^{20})$ to $2.35(10^{20})$ which is still below the experimental value of about $4.3(10^{20})$. Having no independently determined value for n_i at 25°C, we have made no attempt to improve the agreement between these calculated and experimental values.

The value of $4k_s^{1/2}$ is small compared to p-n, approaching a maximum value of 0.4 near 806°C, for Sn-saturated SnTe. The degree of self-compensation defined by Eq. (7) is therefore small in undoped SnTe except near 806°C. Figure 6 shows theoretical isotherms of $|p-n|$ vs $\log P_2$ at 500°C for pure SnTe and for SnTe containing $1.5(10^{20})\text{cm}^{-3}$ of singly-ionized foreign donors. The self-compensation occurring is clearly evident at the higher values of P_2. It is also seen that the theoretical isotherms predict that n-type SnTe can be obtained if a

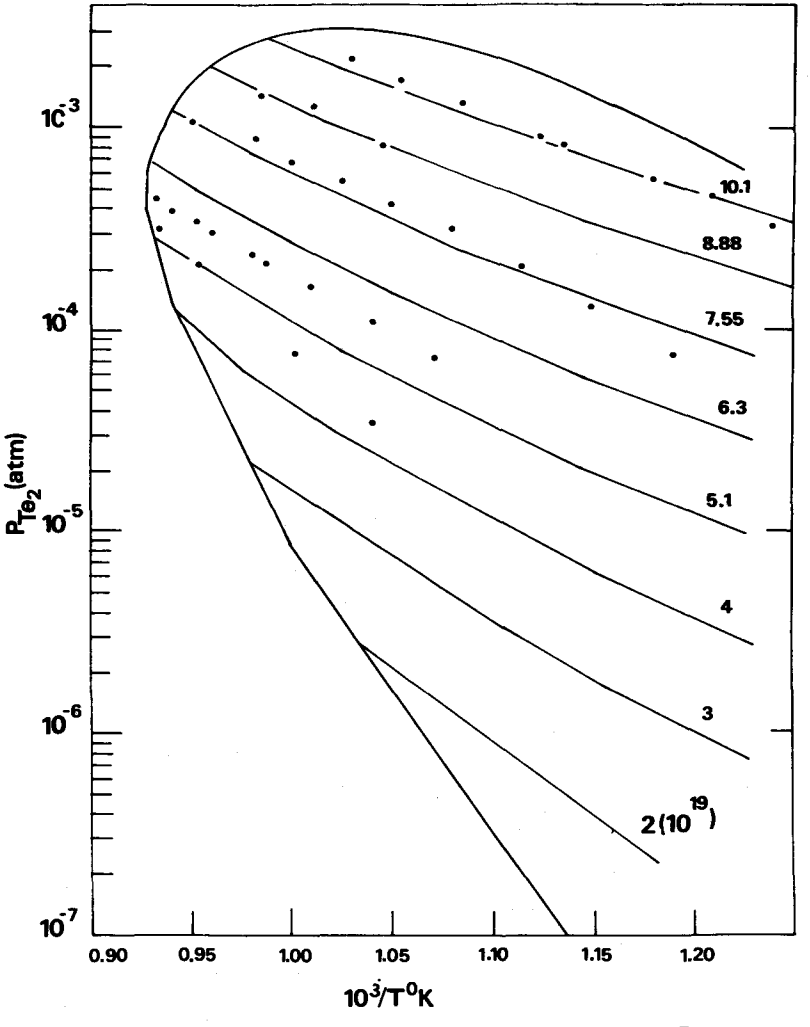

Fig. 5 The partial pressure of Te_2 in atm vs $10^3/T$ for various fixed compositions of SnTe. The experimental data from Ref. 4 are shown as points. The solid lines labeled with the corresponding value of p-n (see Eqs. 22 and 23) were calculated using entry 3, Table VI. The parabola-like solid curve is the experimental partial pressure of Te_2 along the three-phase curve of SnTe which encloses those values of p-n corresponding to compositions of SnTe that are stable at a given temperature.

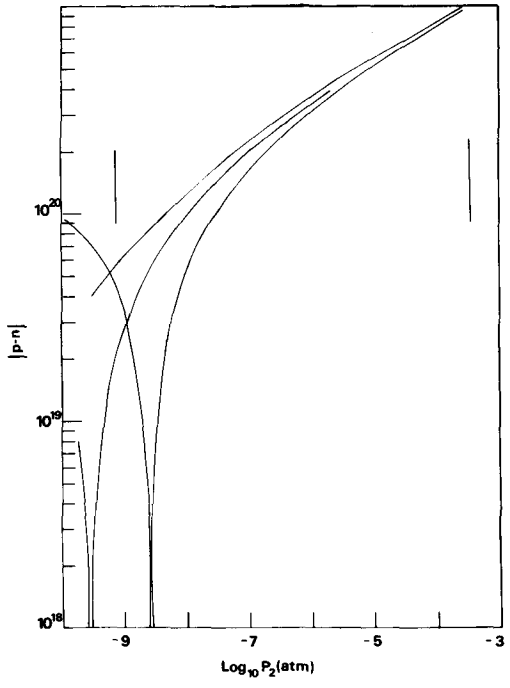

Fig. 6 Calculated 500°C isotherms of p-n for SnTe containing various concentrations of singly-ionized foreign donors plotted on a log scale vs the logarithm of P_{Te_2} in atm. Vertical bars at -9.14 and -3.49 are the values of log P_{Te_2} for, respectively, Sn-saturation and Te-saturation of SnTe. From uppermost to bottom curves at high P_{Te_2}, D = 0, $5(10^{19})$, and $1.5(10^{20})cm^{-3}$.

sufficiently soluble donor can be incorporated into the SnTe without increasing the minimum value of log P_2 for single phase material above the value of -9.14 for pure SnTe.

Summary

Except for Te-saturated points below 370°C, the experimental values of net hole concentration, p-n, and partial pressure of Te_2, P_2, along the Pb and Te-rich solidus lines of PbTe are fit quite closely assuming

either singly or doubly-ionized native defects. Assuming doubly-ionized defects, consistent with recent experiments, and changing the temperature dependence of n_i below 308°C to give a value of $3(10^{15})cm^{-3}$ for n_i at 25°C, leads to a satisfactory fit of the Te-saturated points below 370°C also. As a result the high temperature values for the intrinsic parameters of PbTe, n_i, k_s, and $P_2(int)$ have been established and can be calculated using entry 2 in Table IV.

Similarly the data for SnTe, which include values of p-n, P_2, and T within the homogeneity range of the compound, are fit well except for two compositions for which the experimental results are subject to the greatest uncertainty. The intrinsic parameters, though not precisely established, are close to those calculated using entry 3 in Table VI.

Acknowledgement

The author wishes to thank Dr. B. Houston for furnishing numerical values for his results on Sn-saturated SnTe and for helpful comments, Dr. A. J. Strauss for help in gathering some of the necessary data, and Dr. H. Maier for supplying a preprint of his work on PbSe and drawing attention to that of Dr. Heinrich and co-workers on PbTe. Support of this work from the National Science Foundation under Grant DMR75-09332 is gratefully acknowledged. Finally, thanks are due Barbara Rekowski for typing the manuscript.

Appendix

For calculations such as those performed in this work the computer time required is decreased if an explicit equation for p-n is used such as that given by Eq. (14) of Ref. 13. It is also of interest to show that our Eq. (4) is equivalent to Eq. (14) of Ref. 13 when z = 1. We start somewhat more generally, using Eq. (11), which contains D, the net-concentration of singly-ionized foreign donors,

$$D = \sum_i z[D_i^{+z}] - \sum_j z[A_j^{-z}] ,$$

where $[D_i^{+z}]$ is the concentration of z-fold ionized foreign donors of type i and $[A_j^{-z}]$ is that of z-fold ionized foreign acceptors. The development assumes D is a constant and is unaffected by a changing degree of ionization of the various donors and acceptors. This is not expected to be a good approximation in general, but probably is valid for many impurities in the IV-VI compounds. For compactness let

$$\delta = (p-n)/2n_i \tag{A1}$$

$$\alpha = zk_s^{1/2}/n_i \tag{A2}$$

and $$P_2/P_2(int) = \theta \tag{A3}$$

Then Eq. (11) can be written as

$$\ln \theta^{1/2} = z \sinh^{-1} \delta + \sinh^{-1} \left(\frac{\delta+D}{\alpha}\right) \tag{A4}$$

Solving for the inverse hyberbolic sine of $(\delta+D)/\alpha$ and taking the hyberbolic sine of both sides of Eq. (A4) gives

$$\frac{\delta+D}{\alpha} = \sinh \{\ln \theta^{1/2} - z \sinh^{-1} \delta\} \tag{A5}$$

Using the trigonometric identity for the hyberbolic sine of the difference of two angles and the definitions of the hyberbolic sine and cosine in terms of exponentials, Eq. (A5) can be written as

$$\frac{2(\delta+D)}{\alpha} = \left(\theta^{1/2} - \frac{1}{\theta^{1/2}}\right) \cosh (z \sinh^{-1} \delta) - \left(\theta^{1/2} + \frac{1}{\theta^{1/2}}\right) \sinh (z \sinh^{-1}\delta) \tag{A6}$$

At this point the development for z = 1 and z = 2 proceeds differently.

Case 1. z = 1

Use of the trigonometric identity

$$\cosh u = (1 + \sinh^2 u)^{1/2}$$

allows Eq. (A6) to be written as

$$\frac{2(\delta+D)}{\alpha} = \left(\theta^{1/2} - \frac{1}{\theta^{1/2}}\right)(1+\delta^2)^{1/2} + \left(\theta^{1/2} + \frac{1}{\theta^{1/2}}\right)\delta \qquad \text{(A7)}$$

Solving for $(1+\delta^2)^{1/2}$, squaring both sides of the equation, and solving the resultant quadratic equation in δ gives

$$2(1+\alpha\theta^{1/2})\left(1 + \frac{\alpha}{\theta^{1/2}}\right)\delta = -D\left(2+\alpha\theta^{1/2} - \frac{\alpha}{\theta^{1/2}}\right) + \left[(\alpha D)^2\left(\theta + \frac{1}{\theta} - 2\right) + \left(\alpha\theta^{1/2} - \frac{\alpha}{\theta^{1/2}}\right)(1+\alpha\theta^{1/2})\left(1 + \frac{\alpha}{\theta^{1/2}}\right)\right]^{1/2} \qquad \text{(A8)}$$

This is an explicit equation for δ and therefore for p-n through Eq. (A1).

If D=0, Eq. (A8) reduces to

$$\delta = \frac{\alpha\theta^{1/2} - \frac{\alpha}{\theta^{1/2}}}{2(1+\alpha\theta^{1/2})^{1/2}\left(1 + \frac{\alpha}{\theta^{1/2}}\right)^{1/2}} \qquad \text{(A9)}$$

Using Eqs. (A1) and (A2) to eliminate δ and α and rearranging gives

$$p\text{-}n = \frac{k_s^{1/2} n_i^{1/2}\left(\theta^{1/2} - \frac{1}{\theta^{1/2}}\right)}{\left(n_i + k_s^{1/2}\theta^{1/2}\right)^{1/2}\left(1 + k_s^{1/2}/n_i\theta^{1/2}\right)^{1/2}} \qquad \text{(A10)}$$

Recognizing that $k_s^{1/2}$ is identical to k_d of Ref. 13, Eq. (A10) is identical to their Eq. (13), and, since their n_{77} is taken as n-p, Eq. (A10) is the negative of their Eq. (14).

Case II. z = 2

Using the identities for the hyberbolic sine and cosine of twice an angle in Eq. (A6) with z = 2, and proceeding similarly to before, one obtains a quartic equation for δ:

$$\delta^4 + \frac{1}{2\alpha}\left(\theta^{1/2} - \frac{1}{\theta^{1/2}}\right)\delta^3 + \frac{1}{4}\left[4 - \frac{1}{\alpha^2} + \frac{2D}{\alpha}\left(\theta^{1/2} - \frac{1}{\theta^{1/2}}\right)\right]\delta^2 - \frac{1}{4\alpha}\left(\frac{2D}{\alpha} - \theta^{1/2} + \frac{1}{\theta^{1/2}}\right)\delta - \frac{1}{16}\left(\frac{2D}{\alpha} - \theta^{1/2} + \frac{1}{\theta^{1/2}}\right)^2 = 0 \qquad \text{(A11)}$$

Since the solution of a quartic equation, though complicated, can still be expressed in a finite number of definite steps, it is possible that Eq. (A11) might be useful in shortening computer calculation time compared to that required to solve the implicit equation for p-n (and hence δ) given by either Eq. (4) or Eq. (11).

References

1. R. F. Brebrick and E. Gubner, J. Chem. Phys., 36, 1283 (1962).

2. R. F. Brebrick and A. J. Strauss, J. Chem. Phys., 40, 3230 (1964).

3. R. F. Brebrick, J. Phys. Chem. Solids, 24, 27 (1963).

4. R. F. Brebrick and A. J. Strauss, J. Chem. Phys., 41, 197 (1964).

5. E. M. Logothetis and H. Holloway in "Physics of IV-VI Compounds and Alloys" (Gordon and Breach Science Pub., London, 1974) p. 153.

6. M. Fujimoto and Y. Sato, Jap. J. Appl. Phys., 5, 128 (1966).

7. F. Bis unpublished, Masters Thesis, University of Maryland.

8. H. Heinrich, A. Lopez-Otto, L. Palmetshofer and L. D. Haas, Inst. Phys. Conf. Ser. No. 23.

9. R. F. Brebrick, J. Phys. Chem. Solids, 32, 551 (1971).

10. B. B. Houston, R. S. Allgaier, R. S. Babiskin and P. G. Siebenmann, Bull. Am. Phys. Soc., 9, 60 (1964).

11. R. F. Brebrick in "Progress in Solid State Chem." Vol. 3, Ch. 5, Pergamon Press, Oxford, 1966.

12. R. F. Brebrick, J. Solid State Chem., 1, 88 (1969).

13. T. C. Harman and A. J. Strauss, J. Electron. Mater., 5, 621 (1976).

14. W. W. Scalon, Phys. Rev., 126, 509 (1962).

15. R. F. Brebrick and R. S. Allgaier, J. Chem. Phys., 32, 1826 (1960).

16. R. S. Allgaier and B. B. Houston, Jr., J. Appl. Phys., 37, 302 (1966).

17. A. J. Strauss, J. Electron. Mater., 2, 553 (1973).

18. N. Chou, K. Komarek and E. Miller, Trans. Met. Soc. AIME, 245, 1553 (1969).

19. Y. Sato, M. Fujimoto and A. Kobayashi, Jap. J. Appl. Phys., 2, 688 (1963).

20. R. F. Bis, J. Phys. Chem. Solids, 24, 579 (1963).

21. R. F. Brebrick, J. Phys. Chem., 72, 1032 (1968).

22. D. R. Stull and G. C. Sinke, "Thermodynamic Properties of the Elements" (American Chemical Soc., Wash. D.C. 1956).

23. J. H. McAteer and H. Seltz, J. Am. Chem. Soc., 58, 208 (1936).

24. H. T. Savage, B. Houston and J. R. Burke, Phys. Rev. B, 6, 2292 (1972).

25. J. A. Nelder and R. Mead, Computer J., 7, 308 (1965).

26. I. Melngailis and T. C. Harman, "Semiconductors and Semimetals", R. K. Willardson and A. C. Beer, Eds. (Academic Press, New York 1970) Vol. 5, p. 160.

27. R. Dalven, Infrared Phys., 9, 141 (1969).

28. H. Maier, D. R. Daniel and H. Preier, J. Crystal Growth, 35, 121 (1976).

29. J. Bloem and F. A. Kroger, Z. physik. Chem., 7, 1 (1956).

30. N. Ohashi, Trans. Jap. Inst. Metals, 5, 94 (1964).

31. A. V. Novoselova, V. P. Zlomanov and O. V. Matveev, Izv. Akad. Nauk SSR, Neorgan. Materialy, 3, 1323 (1967).

32. A. M. Gas'kov, O. V. Matveev, V. P. Zlomanov and A. V. Novoselova, Izv. Akad. Nauk. SSR, Neorg. Mater., 5, 1889 (1969).

33. A. V. Novoselova, V. P. Zlomanov, S. G. Karbanov, O. V. Matveev and A. M. Gas'kov in "Progress in Solid State Chemistry" Vol. 7, Ch. 3, Edited by H. Reiss and J. O. McCaldin, Pergamon Press (1972).

34. A. M. Gas'kov, V. P. Zlomanov and A. V. Novoselova, Vest. Mosk. Univ., Khimii, 11, 49 (1970).